


RESEARCH ARTICLE

Reaction Engineering, Kinetics and Catalysis

Quantifying molecular surface barriers and intracrystalline diffusion in nanoporous materials by zero-length column

Yiwei Xie^{1,2} | Hua Li¹  | Caiyi Lou^{1,2} | Mao Ye¹  | Zhongmin Liu^{1,2}

¹National Engineering Research Center of Lower-Carbon Catalysis Technology, Dalian National Laboratory for Clean Energy, Dalian Institute of Chemical Physics, Chinese Academy of Sciences, Dalian, China

²University of Chinese Academy of Sciences, Beijing, China

Correspondence

Hua Li and Mao Ye, Dalian Institute of Chemical Physics, Chinese Academy of Sciences, Dalian 116023, Liaoning, China.
Email: lihua@dicp.ac.cn and maoye@dicp.ac.cn

Funding information

National Natural Science Foundation of China, Grant/Award Numbers: 22293021, 21991093, 22288101; Strategic Priority Research Program of the Chinese Academy of Sciences, Grant/Award Number: XDA21030200

Abstract

The zero-length column (ZLC) method has been frequently used to measure the effective diffusivity of guest molecules in nanoporous crystalline materials. Recent studies unveiled that the mass transport of guest molecules could originate from either intracrystalline diffusion and/or surface barriers. Directly quantifying the intracrystalline diffusivity and surface permeability of guest molecules, therefore, is essential for understanding the mass transfer and thus optimizing the design of nanoporous crystalline materials. In this work, we extended the ZLC method, based on a derived theoretical expression of the desorption rate, to decouple the surface barriers and intracrystalline diffusion from effective diffusion of guest molecules in nanoporous materials. The diffusivities of ethane, propane and n-pentane in SAPO-34 and Beta zeolites have been experimentally measured to verify the effectiveness of this method.

KEYWORDS

intracrystalline diffusion, mass transfer, nanoporous materials, surface barriers, zero-length column

1 | INTRODUCTION

Nanoporous crystalline materials are widely used in the industrial catalysis,^{1,2} gas separation,^{3,4} and emerging energy technologies.⁵ The mass transfer of guest molecules in nanoporous materials is of fundamental importance because it is related to, for example, the catalytic reaction activity^{6,7} and separation performance.^{8–10} Therefore, the rational design and efficient utilization of nanoporous crystalline materials require in-depth understanding of the underlying mass transport phenomena.^{11,12} Many studies have shown that there exist two mechanisms for mass transport resistance of guest molecules in nanoporous crystals, that is, the intracrystalline diffusion resistance and surface barriers.^{13–22} Both mechanisms could dominate the mass transfer of guest molecules in nanoporous materials^{23–28} though they have quite different origins. The intracrystalline diffusion is mainly affected by the interaction between host and guest molecules as well as the topological structure of the materials,^{26,29} while the surface barriers originated from blockage of surface pores^{23,27,28} or the large

energy difference of guest molecules between gas/fluid phase and adsorbent space.^{30–32} Quantifying these two mechanisms presents a key challenge in the industrial applications of nanoporous crystalline materials.

In a recent work, a theoretical method has been proposed to distinguish the intracrystalline diffusivity and surface permeability using the adsorption data measured by intelligent gravimetric analyzer (IGA).³³ Note that the zero-length column (ZLC) technology, which was first developed by Eic and Ruthven,^{34,35} represents a versatile yet easily accessible approach that has been widely used for studying the diffusivity of guest molecules in nanoporous materials,^{36–39} the purpose of this paper is to establish a theoretical approach to quantify the respective contributions of intracrystalline diffusion and surface barriers to overall effective diffusivity^{6,40} measured by ZLC.

In the ZLC technology, an inert gas is purged to desorb the target gas molecules preabsorbed in a small well-mixed sample at certain partial pressure. Thus the effective diffusivity measured by ZLC is essentially based on the desorption rate curves. Conventionally

variable separation has been considered as a main approach to derive the diffusivity by solving the diffusion equation. In a contribution Ruthven et al.⁴¹ tried to estimate the surface permeability by use of the variable separation to obtain the intercepts with different sets of purge rates based on the long-time method. This was an interesting attempt to decouple surface barriers from the intracrystalline diffusion. Here, we derived an analytical expression of surface permeability through the Laplace transform of the governing equation describing the desorption of guest molecules in ZLC cell. In this way, we can offer a direct way to simultaneously obtain surface permeability and intracrystalline diffusivity of guest molecules by use of ZLC, which is expected to favor the understanding of mass transfer mechanisms in nanoporous materials.

2 | THE MODEL

As shown in Figure 1A, a sample of nanoporous materials is packed in the ZLC cell. The mass transfer during the desorption of guest molecules in nanoporous materials, under the assumption of Fick's law,⁴² can be described as

$$\frac{\partial q}{\partial t} = D \frac{\partial^2 q}{\partial x^2} \quad (1a)$$

where q (kmol/m³) is the loading of adsorbate molecules in nanoporous materials, t (s) is the time, D (m²/s) is the intracrystalline diffusivity and x (m) is the Cartesian coordinates. And the initial and boundary conditions are

$$q|_{t=0} = q_0 \text{ for all } x \quad (1b)$$

$$D \frac{\partial q}{\partial x} \Big|_{x=l} = \alpha (fc - q|_{x=l}) \quad (1c)$$

$$\frac{\partial q}{\partial x} \Big|_{x=0} = 0 \quad (1d)$$

where q_0 (kmol/m³) is the value of q at initial steady state, α (m/s) is the surface permeability, l (m) is the half thickness of the nanoporous materials in the shape of a plane sheet, that is, the characteristic length of the intracrystalline diffusion, f (dimensionless) is the dimensionless Henry constant, and c (kmol/m³) is concentration of adsorbate molecules in the gas phase.

By purging carrying gas, the adsorbate molecules are desorbed from the nanoporous materials. Considering the thin bed of nanoporous materials with a relatively large velocity of gas, we can assume the adsorbent molecules are perfectly mixed, and the concentration could reach equilibrium quickly. Then the concentration of adsorbate molecules in the carrying gas can be described as.

$$\frac{dc}{dt} = -k_f \cdot c - \frac{D}{h} \frac{\partial q}{\partial x} \Big|_{x=l} \quad (2)$$

which can be reduced to

$$c = - \frac{D}{k_f \cdot h} \frac{\partial q}{\partial x} \Big|_{x=l} \quad (3)$$

suppose that $dc/dt = 0$. Here k_f (1/s) represents the ratio of the volume of purging gas to the void fraction of the bed. Note that $h = V_p \cdot \varepsilon / S_p / (1 - \varepsilon)$, where ε (dimensionless) is the void fraction of the bed, and V_p (m³) and S_p (m²) are the total volume and area of crystals, respectively.

From Equation (2), we can replace c in Equation (3) with $\frac{\partial q}{\partial x} \Big|_{x=l}$. Then Equation (1) could be rewritten in the dimensionless form:

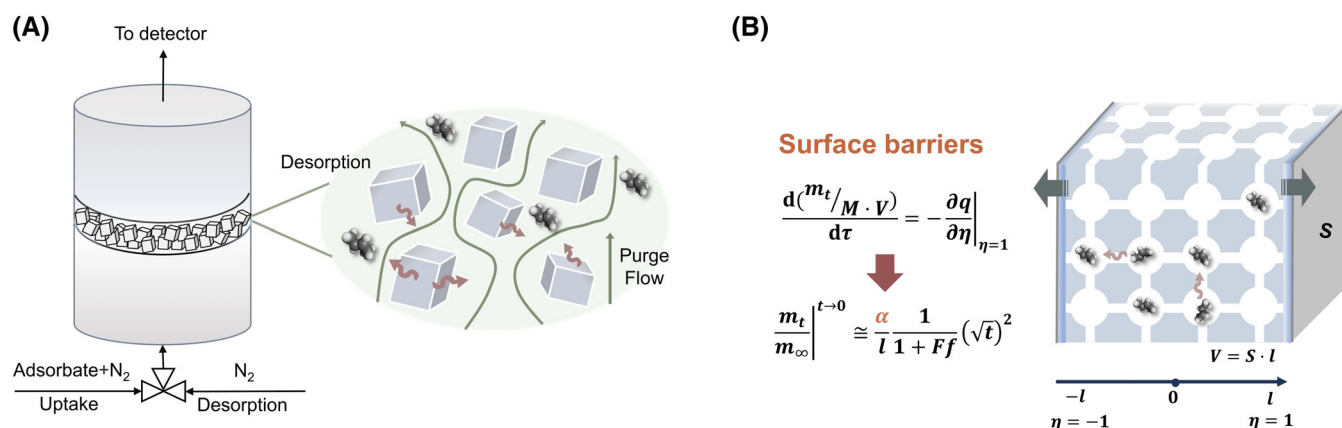


FIGURE 1 (A) Schematics of the ZLC experimental arrangement for mass transfer studies in nanoporous solids: The nanoporous material installed in the ZLC column is assumed to be in the shape of a half-plate. (B) The guest molecules are desorbed from the inside and need to experience the limitations of intracrystalline diffusion (pores and cages) and surface interface barriers (blue-gray at the edges of the material). Here, our experiments are all under low loading of adsorbates, and molecular interactions can be ignored.

$$\begin{cases} \frac{\partial q}{\partial \tau} = \frac{\partial^2 q}{\partial \eta^2} & (4a) \\ \left. \frac{\partial q}{\partial \eta} \right|_{\eta=0} = 0 & (4b) \\ \left. \frac{\partial q}{\partial \eta} \right|_{\eta=1} = -\frac{L}{1+F} q|_{\eta=1} = -H \cdot q|_{\eta=1} & (4c) \\ q|_{\tau=0} = q_0 & (4d) \end{cases}$$

Note that the dimensionless quantities above are defined as $\tau = \frac{D t}{l^2}$, $F = \frac{\alpha}{k h}$, $H = \frac{L}{1+F}$, and $L = \frac{d}{D}$. Here L implies the ratio of characteristic time of intracrystalline diffusion to that of surface permeability. Equation (4) can be solved by using the method of separation of variables

$$\frac{q(\eta, \tau)}{q_0} = \sum_{n=1}^{\infty} \frac{4 \sin(\beta_n)}{2\beta_n + \sin(2\beta_n)} \cdot \exp(-\beta_n^2 \tau) \cos(\beta_n \eta) \quad (5a)$$

$$\beta_n \tan(\beta_n) = H \quad (5b)$$

where β_n is calculated by the roots of the transcendental equation Equation (5b). The derivation of the solution, Equation (5a), can also be found in "The Mathematics of Diffusion"⁴³ by J. Crank (second edition, p. 60, Equation 4.50).⁴³ But here our solution can be considered as a special case specifically for ZLC measurements by assuming $q_e = 0$. Finally, the expression of the ZLC desorption curve can be obtained (for the detailed derivation process, see Supporting information),

$$\frac{c(t)}{c_0} = 1 - \sum_{n=1}^{\infty} \frac{2L^2}{\beta_n^2 (\beta_n^2 + L^2 + L)} \exp\left(-\beta_n^2 \frac{D}{l^2} t\right) \quad (6)$$

where $c(t)$ (kmol/m³) is the concentration of adsorbate molecules in the gas flowing out of the ZLC cell at time t , c_0 (kmol/m³) is the value of $c(t)$ at initial steady state, $c(t)/c_0$ is the normalized concentration at the release time t . It can be seen from Equations (5) and (6) that the solution of the desorption amount obtained by the variable separation method contains the combined resistance caused by both intracrystalline diffusivity and surface barriers, which are respectively described by intracrystalline diffusivity and surface permeability. Thus, effect of either the intracrystalline diffusion or surface barriers cannot be directly quantified solely using Equation (6).

We further consider a solution suitable for small t by expanding the expression using the Laplace transform in a series of negative exponents⁴⁴ (see detailed derivation of Equations (7)–(17) in Supporting Information). By applying the Laplace transform to Equation (4), we can obtain:

$$\begin{cases} \frac{d^2 Q}{d\eta^2} - Q \cdot s + q_0 = 0 & (7a) \\ \left. \frac{dQ}{d\eta} \right|_{\eta=0} = 0 & (7b) \\ \left. \frac{dQ}{d\eta} \right|_{\eta=1} = -H \cdot Q|_{\eta=1} & (7c) \end{cases}$$

Here Q is used to replace q as in Equation (4):

Then, we can derive the solution:

$$Q = \frac{q_0}{s} - \frac{q_0}{s} \cdot \frac{H \cdot [\exp(\sqrt{s}\eta) + \exp(-\sqrt{s}\eta)]}{(H + \sqrt{s}) \cdot \exp(\sqrt{s}) + (H - \sqrt{s}) \cdot \exp(-\sqrt{s})} \quad (8)$$

Equation (8) can also be written as

$$\begin{aligned} \frac{Q}{q_0} = & \frac{1}{s} - \frac{H \cdot [\exp[-(1-\eta)\sqrt{s}] + \exp[-(1+\eta)\sqrt{s}]]}{s \cdot (H + \sqrt{s})} \\ & \cdot \sum_{n=0}^{\infty} (-1)^n \left(\frac{H - \sqrt{s}}{H + \sqrt{s}} \right)^n \exp(-2n\sqrt{s}) \end{aligned} \quad (9)$$

When only the first term ($n = 0$) is considered, the above equation becomes

$$\frac{Q}{q_0} = \frac{1}{s} - \frac{H}{s(H + \sqrt{s})} [\exp[-(1-\eta)\sqrt{s}] + \exp[-(1+\eta)\sqrt{s}] + \dots] \quad (10)$$

According to the inverse Laplace transform,

$$\begin{aligned} \mathcal{L}^{-1} \left\{ \frac{H \exp(-k\sqrt{s})}{s(H + \sqrt{s})} \right\} = & -\exp(Hk + H^2 \tau) \cdot \operatorname{erfc} \left(H\sqrt{\tau} + \frac{k}{2\sqrt{\tau}} \right) \\ & + \operatorname{erfc} \left(\frac{k}{2\sqrt{\tau}} \right) \frac{dQ}{d\eta} \Big|_{\eta=0} \\ = & 0 \end{aligned} \quad (11)$$

we can obtain the loading of adsorbate molecules at initial stage (i.e., a small t)

$$\begin{aligned} \frac{Q}{q_0} = & \frac{1}{s} - \frac{H}{s(H + \sqrt{s})} \left[\sum_{n=0}^{\infty} (-1)^n \left(\frac{H - \sqrt{s}}{H + \sqrt{s}} \right)^n \exp[-(-2n+1-\eta)\sqrt{s}] \right. \\ & \left. + \sum_{n=0}^{\infty} (-1)^n \left(\frac{H - \sqrt{s}}{H + \sqrt{s}} \right)^n \exp[-(-2n+1+\eta)\sqrt{s}] \right] \end{aligned} \quad (12)$$

Since at the boundary we have $\eta = 1$, the expression of q at initial stage becomes

$$\begin{aligned} \frac{q|_{\eta=1}}{q_0} = & 1 - \left[1 - \exp(H^2 \tau) \cdot \operatorname{erfc}(H\sqrt{\tau}) + \operatorname{erfc} \left(\frac{2}{2\sqrt{\tau}} \right) \right. \\ & \left. - \exp[2H + H^2 \tau] \cdot \operatorname{erfc} \left(H\sqrt{\tau} + \frac{2}{2\sqrt{\tau}} \right) \right] \end{aligned} \quad (13)$$

Note that Equations (11) and (13) are valid only when time τ (or t) is small, the Equation (13) can be further simplified to

$$\frac{q|_{\eta=1}^{\tau \rightarrow 0}}{q_0} = 1 - \left[1 - \exp(H^2 \tau) \cdot \operatorname{erfc}(H\sqrt{\tau}) \right] = \exp(H^2 \tau) \cdot \operatorname{erfc}(H\sqrt{\tau}) \quad (14)$$

As shown in Figure 1B, the desorption of adsorbate molecules can be alternatively described in differential form as (see details in Supporting information)

$$\frac{d(m_t/M \cdot V)}{d\tau} = \frac{\partial q}{\partial \eta} \bigg|_{\eta=1} \quad (15)$$

Here, m_t (kg) is the mass of adsorbate molecules desorbed from nanoporous materials at time t , M (kg/m³) is the molar mass of adsorbate molecules, and V (m³) is the volume of the half plane sheet. A solution of outflow mass can be obtained (see detailed derivation of Equation (S50) in Supporting information):

$$\frac{m_t}{m_\infty} = \sqrt{\frac{4\tau}{\pi}} - \frac{1 - \exp(H^2\tau) \operatorname{erfc}(H\sqrt{\tau})}{H} \quad (16)$$

Expanding Equation (16) by Taylor series of variable $\sqrt{\tau}$ (for detailed derivation, see Supporting information), we obtain

$$\frac{m_t}{m_\infty} \bigg|^{t \rightarrow 0} \cong \frac{\alpha}{l} \frac{1}{1 + F\tau} (\sqrt{t})^2 \quad (17)$$

with $F = \frac{\alpha}{k_p h}$. Here m_t/m_{total} is the normalized loading of the adsorbate molecules desorbed from nanoporous materials at time t .

In Equation (17), through Laplace transform, the intracrystalline diffusivity and the surface permeability can be easily decoupled, compared to Equation (6) obtained by the method of separation of variables. The outflow mass at the initial stage of desorption is dominantly controlled by the surface barriers with negligible effect of intracrystalline diffusion. A further check shows that m_t/m_∞ is actually a quadratic function of the square root of desorption time. Meanwhile, the quadratic term coefficient is related to the surface permeability, the size of samples, the desorption gas velocity and the Henry constant. Except for the surface permeability, other parameters can be obtained in advance; The desorption gas velocity is set experimentally, and the Henry constant is obtained from the isotherm adsorption curve (see Supporting information for details). Therefore, according to Equation (17), the zero-length column technique can directly quantify the surface barriers of adsorbate molecules of mass transfer in nanoporous materials. The normalized effluent mass is obtained by integrating the concentration curve (ZLC measurement) against time. Then, the surface permeability is determined by fitting the initial normalized outflow mass curves to Equation (17). In practice, due to the effect of dead volume, the appropriate desorption initiation moment needs to be chosen based on the criterion that the fitted curve has the maximum coefficient of determination with the experimental data. Ultimately, the whole desorption curve can be further fitted to obtained intracrystalline diffusivity with Equation (6).

In this way, the desorption curves of ZLC can be used to directly obtain the surface permeability and intracrystalline diffusivity with well-defined physical meanings using the decoupled surface diffusion and intracrystalline diffusion models. Note that a constant temperature of system was assumed in the derivation above. The temperature of ZLC cell, therefore, should maintain unchanged in the real

experiments, and thus we can ignore the temperature variation during the mass transfer process of guest molecules in nanoporous materials.

3 | EXPERIMENTAL METHOD

3.1 | Sample synthesis and characterizations

Two SAPO-34 samples were used for experimental measurement, which were named SAPO-34-7 μm and SAPO-34-2 μm according to the size of crystal, respectively. The synthesis procedures of SAPO-34-7 μm used in the experiments were reported in previous work.⁴⁵ The SAPO-34-2 μm was purchased from Catalyst & Catalysis Technology Company, Dalian, China. X-ray diffraction pattern (XRD) of the samples were obtained by powder X-ray diffraction on a PANalytical X'Pert PRO x-ray diffractometer operating at 40 mA and 40 kV with Cu Kα radiation ($\lambda = 0.154059$ nm) in the 2θ range from 5° to 40°. The morphological characteristics and crystal sizes of SAPO-34 samples were recorded by using a Hitachi SU8020 field emission scanning electron microscope. The nitrogen adsorption-desorption isotherms at 77 K were measured by Micromeritics ASAP 2020. The samples were degassed at 673 K for 6 h under vacuum to remove adsorbed moisture. The surface area, total pore volume, and micropore volume were calculated by Brunauer-Emmett-Teller (BET) and t-plot methods. The adsorption isotherm of the ethane on the sample was measured by Micromeritics Gemini 2390. The samples were placed at 623 K for 6 h under nitrogen flow to remove adsorbed moisture. The chemical composition of each SAPO-34 sample was determined with a Philips Magix-601 spectrometer. The temperature-programmed desorption (TPD) profiles of ammonia were recorded on a chemical adsorption instrument, namely Micrometric 2920. For experimental operations, 100 mg the sample of 40–60 mesh was heated for 1 h at 873 K in a quartz U-shaped reaction tube under He gas flow. Then the sample is saturated with ammonia until the temperature drops to 373 K. Next the NH₃-TPD was executed at a constant rate of 10 K/min from 373 to 873 K. The details and data processing of diffusion measurement for the samples are detailed in Supporting information.

3.2 | ZLC experiment

The release rates of adsorbates on the samples were measured by the ZLC technology. Prior to the measurements, the sample was activated in N₂ flow (80 mL/min) at 473 K for 8 h. Then, the adsorbate molecules under the dilution of N₂ were introduced into the ZLC cell until the porous materials were saturated with the adsorbate molecules by adsorption. After the adsorption of adsorbates on the sample reached equilibrium, the four-way valve was switched to purge N₂ into the ZLC cell, and adsorbate molecules were introduced into the flame ionization detector (FID). Meantime the transient outflow concentration was recorded. The ZLC cell is operated at ambient pressure and varying temperature. Three measuring temperatures were used for

propane (303, 313, and 333 K) and one for ethane (303 K). Based on the method we developed above, we can directly quantify the surface barriers in the sample, which can be further used to obtain the intracrystalline diffusivity by fitting the overall desorption ZLC curve (see Supporting information for details).

4 | RESULTS AND DISCUSSION

4.1 | Validation of the model at different gas velocities

In Equation (17), the initial normalized desorption rate is related to the velocity of purge gas. Here, the diffusion of propane in SAPO-34-2 μm zeolites measured by ZLC, different velocities of purge gas were set to quantify diffusion to validate the model. As shown in Figure 1 and Table 1, similar surface permeability and intracrystalline diffusivity were obtained at different velocities, the deviation of the measurement result from the average value is within 2%. In Equation (17), when the gas velocity increases, the coefficient of the quadratic term of the initial desorption curve increases. The experimental data shows this trend and can be well fitted by Equation (17), thus verifying applicability of Equation (17) at different gas velocities. The results of diffusion show that surface barriers are determined by the host-guest interaction independent of the velocity of purge gas. Under the current gas velocity, the effect of external diffusion on the measurement can be excluded, and stable results can be obtained by developed method (Figure 2).

4.2 | Diffusion of ethane on SAPO-34 quantified by various methods

In previous studies, the effective diffusivity measured by macroscopic techniques, for example, ZLC technique often has a gap of nearly one order of magnitude with that measured by microscopic techniques. In order to reveal the reasons underlying the gap between macro- and micromasurement techniques, and improve the credibility of the measurement results of ZLC method, the diffusion of ethane in SAPO-34-7 μm was measured by the ZLC technique (303 K) and PFG NMR technique (298 K) respectively. The initial (Figure 3A) and overall curves (Figure 3B) of the desorption efflux can be well fitted by Equations (17) and (6), respectively, to obtain the surface permeability and

intracrystalline diffusivity. As shown in Figure 3C, the effective diffusivity obtained by the long-time method³⁵ is $1.84 \times 10^{-13} \text{ m}^2/\text{s}$, which is significantly lower than the intracrystalline diffusivity. Generally, the effective diffusivity can be calculated by^{8,20,27,33}

$$\frac{1}{D_{\text{eff}}} = \frac{1}{D} + \frac{3}{al} \quad (18)$$

Thus the effective diffusivity of ethane in SAPO-34-7 μm zeolites obtained by Equation (18) is $1.39 \times 10^{-13} \text{ m}^2/\text{s}$, which shows that the surface barriers constitute the main reason for the significantly lower effective diffusivity. Furthermore, we used PFG NMR technology to measure ethane in this sample, and showed that the self-diffusivity is $D = 5.1 \times 10^{-12} \text{ m}^2/\text{s}$. The intracrystalline diffusivity with decoupled surface barriers obtained from Equation (17) is slightly smaller than the self-diffusivity, which is in the same order of magnitude. In this experiment, the gap between the two is speculated to be caused by different loads. The zero-length column requires a very low load, and the NMR maintains a 60% ethane atmosphere (40% nitrogen) to ensure peak signal strength. In the work of Bonilla et al.,⁴⁶ the surface permeability of ethane on SAPO-34 is measured as $5.67 \times 10^{-7} \text{ m}^2/\text{s}$, which is of the same order of magnitude as our results. Due to the diversity of surface barriers between crystals,^{27,47} the surface permeability obtained by the macroscopic technology is the result of statistical average of multiple grains, which is speculated to be the reason for the difference in surface permeability measured by macroscopic and microscopic technique. Since the macroscopic method is still a better choice for measuring small-sized crystals with the industry interests (the requirements of optical testing methods for size of crystals are usually within $\sim 50 \mu\text{m}$ ²⁶). The reasons for the gap between the measurement techniques obtained by the microscopic and the macroscopic need to be further discussed. One possible reason is that different methods might only be suitable for diffusion with certain characteristic time.^{48,49} For example, there are extensive studies on the differences of diffusivities between PFG-NMR and molecular dynamics results. The diffusion processes that can be measured by PFG NMR normally have observation time of the order of ms. Thus the diffusivity measured by PFG NMR is typically from 10^{-8} to $10^{-12} \text{ m}^2/\text{s}$. The diffusivity measured by ZLC, however, generally is in the range of 10^{-10} to $10^{-15} \text{ m}^2/\text{s}$.⁵⁰ Still, it can be seen from the results that the decoupling of surface barriers can greatly reduce the gap of diffusivity measured by microscopic and macroscopic methods, indicating that the contribution of the surface barriers to the overall diffusion cannot be ignored.

4.3 | Diffusion of propane in SAPO-34 of adsorption and desorption

Although molecular simulation results have shown the effect of surface barriers of adsorption and desorption is symmetry,¹⁹ the issue is controversial due to insufficient understanding of the origins of surface barriers and the lack of intuitive and systematic experimental

TABLE 1 Surface permeability and intracrystalline diffusivity of propane in SAPO-34-2 μm at 313 K measured with different velocities of purge gas.

| The velocity of purge (mL/min) | Surface permeability (m/s) | Intracrystalline diffusivity (m^2/s) |
|--------------------------------|----------------------------|--|
| 55 | 2.88×10^{-09} | 2.80×10^{-16} |
| 60 | 2.86×10^{-09} | 2.84×10^{-16} |
| 71 | 2.86×10^{-09} | 2.94×10^{-16} |

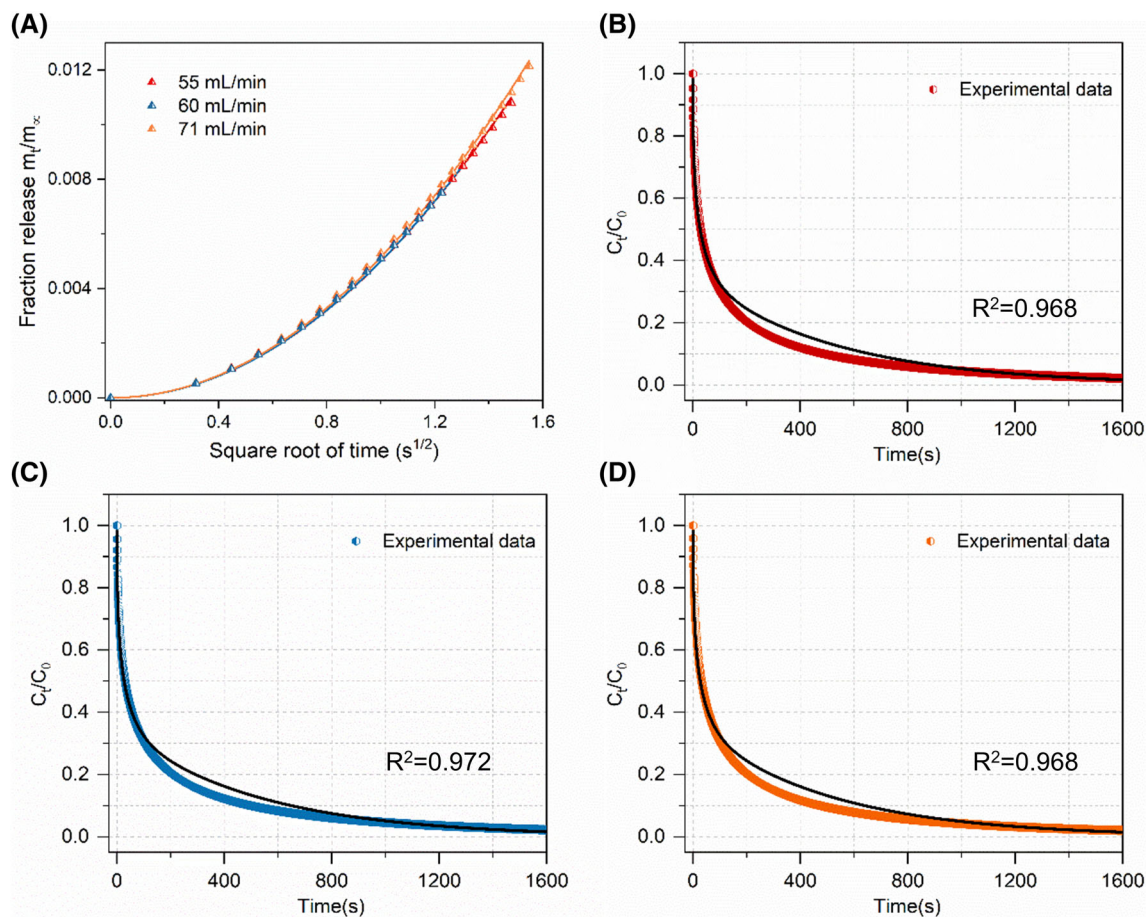


FIGURE 2 (A) Initial normalized outflow of mass and (B–D) overall ZLC desorption curves of propane in SAPO-34-2 μm with different velocities of purge (B), 55 mL/min; (C), 60 mL/min; (D), 71 mL/min. The scatters represent the experimental data while solid lines are fitting results by Equation (17) (A) and Equation (6) (B–D). R^2 represents the coefficient of determination.

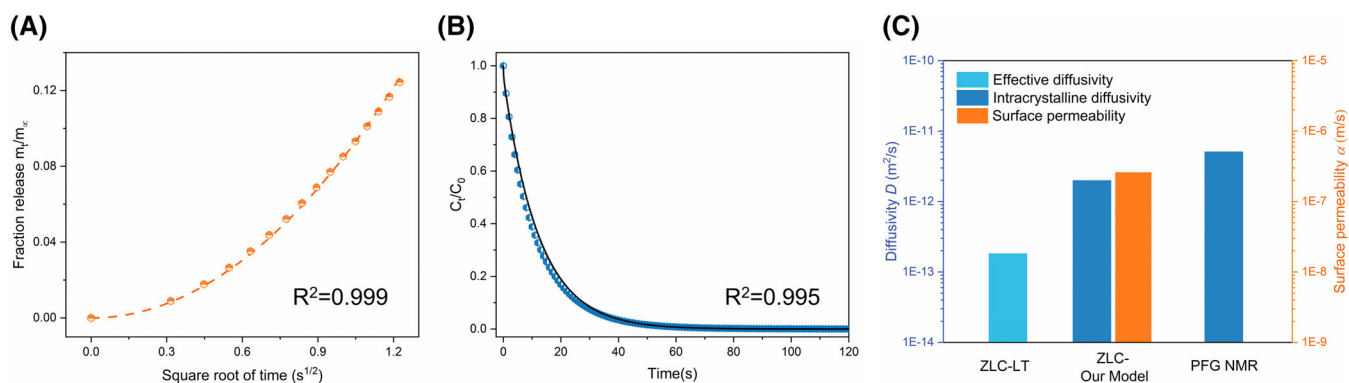


FIGURE 3 (A,B) Initial normalized outflow of mass (A) and overall ZLC desorption curves (B) of ethane in For peer review only SAPO-34 (7 μm). (C) Diffusivities of ethane in SAPO-34 zeolites measured by ZLC and PFG NMR techniques. The effective diffusivity and self-diffusivity are obtained by long-time method of ZLC (ZLC-LT) and PFG NMR.

evidence. Here, surface barriers of the desorption process of propane in SAPO-34-2 μm zeolites at different temperatures was quantified by our method measured by ZLC technique and compared with the results of the adsorption process measured by IGA technique.³³ Figure 4 shows the decoupled intracrystalline diffusivity and surface

permeability obtained by ZLC and IGA techniques at 303, 313, and 333 K, respectively. The experimental results demonstrate that the two measurement techniques obtain basically the same intracrystalline diffusivity, and it is consistent with the results of Cai et al.,⁵¹ which further confirms accuracy of measurement performed by

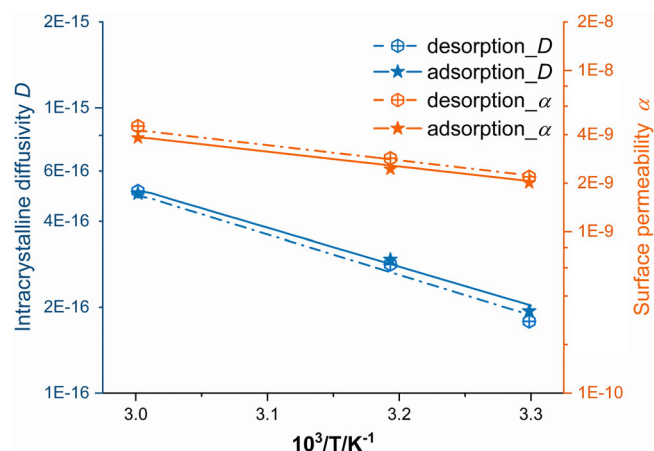


FIGURE 4 Surface permeability and intracrystalline diffusivity of propane in SAPO-34 (2 μm). The diffusion of adsorption and desorption are measured by IGA (filled symbols) and ZLC (open symbols) techniques, respectively.

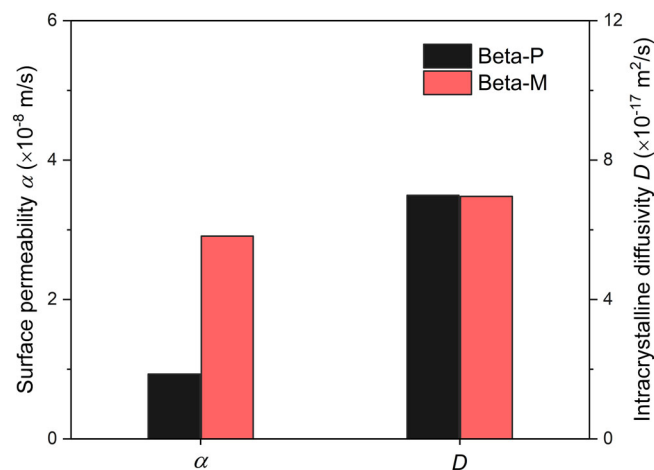


FIGURE 5 Diffusivity of n-pentane measured by ZLC using our method. Beta-P, parent sample; Beta-M, SiO_2 -modified sample.

developed method. For surface permeability, the values obtained by the two techniques are also basically equal, which indicates that surface barriers of diffusion of propane in SAPO-34 is basically symmetrical. Though, more systematic and detailed experiments are still required to confirm the symmetry of the surface resistance. From this matter, the developed method can be used to quantify the surface barriers of desorption processes, such as product molecules that are closely related to selectivity.

4.4 | Diffusion of n-pentane in beta zeolites quantified by current method

To further expand the generalizability of the method, data already reported in the article is reprocessed. In a recent work Hu et al.⁴⁰ carefully modified the surface properties of beta zeolites and

expected that the surface modification could increase surface permeability and thus improve the catalytic efficiency of the isomerization of n-pentane. In this work, ZLC was used to measure the diffusion of beta zeolites with different surface barriers. In the absence of methods to decouple surface permeability and intracrystalline diffusivity, they only measured the effective diffusivity using the long-time method, which cannot clearly distinguish the role of surface barriers from effective diffusivity. Here, we reprocessed their experimental data using our proposed method. In Figure 5, the respective changes of surface permeability and intracrystalline diffusivity can be obtained. As can be seen, the surface permeability of the sample (red) deposited by silica has nearly doubled, and the intracrystalline diffusivity keeps almost unchanged. This provides a direct explanation on how the modification of mass transfer property of the crystal surface affects the reaction performance.

5 | CONCLUSIONS

In this paper, we derived a theoretical expression of desorption curve of guest molecules in nanoporous crystalline materials based on molecular transport theory. As this expression is dependent only on the surface permeability, it is thus possible to apply the widely used ZLC method to decouple the surface barriers and intracrystalline diffusion in mass transport of guest molecules.

We experimentally studied the diffusion of ethane in SAPO-34 zeolites and it is shown that intracrystalline diffusivity measured by ZLC is consistent with that by PFG NMR techniques. In addition, we used IGA (the adsorption rate) to study the diffusion of propane in SAPO-34, which demonstrates that both intracrystalline diffusivity and surface permeability measured by IGA agree well with those measured by ZLC, respectively, for the temperature ranging from 303 to 333 K. Apparently, the ZLC method can be used as an effective measurement technique to quantify the surface barriers and intracrystalline diffusion in nanoporous materials.

Note that surface barriers and intracrystalline diffusion represent two most important mass transfer mechanisms of guest molecules in nanoporous crystalline materials with quite different originalities, directly quantifying these two mechanisms using ZLC opens a potential approach for either fundamental understanding of the mass transport in nanoporous materials or practical improvement of heterogeneous catalysis and gas separation of industrial interests.

AUTHOR CONTRIBUTIONS

Yiwei Xie: Data curation (lead); formal analysis (lead); investigation (lead); methodology (equal); validation (lead); writing – original draft (lead). **Caiyi Lou:** Validation (supporting); writing – original draft (supporting). **Mao Ye:** Conceptualization (equal); data curation (supporting); formal analysis (supporting); funding acquisition (lead); methodology (supporting); project administration (equal); resources (supporting); supervision (lead); writing – review and editing (lead). **Zhongmin Liu:** Conceptualization (supporting); funding acquisition

(lead); project administration (lead); resources (supporting); supervision (equal). **Hua Li**: Formal analysis (supporting); methodology (supporting); supervision (equal); writing – original draft (supporting); writing – review and editing (lead).

ACKNOWLEDGMENTS

This work was supported by the National Natural Science Foundation of China (Grant No. 22293021, 21991093, 22288101), and Strategic Priority Research Program of the Chinese Academy of Sciences (Grant No. XDA21030200). We greatly appreciate Prof. Guanghua Ye of East China University of Science and Technology for the provision of data of n-pentane diffusion in beta zeolites measured by ZLC. The authors thank Prof. Miao Yang in Dalian Institute of Chemical Physics, Chinese Academy of Sciences for the help with synthesis of SAPO-34 zeolites.

DATA AVAILABILITY AND REPRODUCIBILITY STATEMENT

The numerical data from Figures 3C, 4 and 5 are tabulated in Table S2 in Supporting information. Numerical data for the initial normalized outflow of mass and overall ZLC desorption curves from Figures 2 and 3A,B are available as a Data of the artical.zip file in the Supporting information.

ORCID

Hua Li  <https://orcid.org/0000-0003-3291-7844>

Mao Ye  <https://orcid.org/0000-0002-7078-2402>

REFERENCES

- Olsbye U, Svelle S, Bjrgen M, et al. Conversion of methanol to hydrocarbons: how zeolite cavity and pore size controls product selectivity. *Angew Chem Int Ed*. 2012;51(24):5810-5831.
- Weckhuysen BM, Yu J. Recent advances in zeolite chemistry and catalysis. *Chem Soc Rev*. 2015;44(20):7022-7024.
- Rangnekar N, Mittal N, Elyassi B, Caro J, Tsapatsis M. Zeolite membranes—a review and comparison with MOFs. *Chem Soc Rev*. 2015;44(20):7128-7154.
- Bereciartua PJ, Cantin A, Corma A, et al. Control of zeolite framework flexibility and pore topology for separation of ethane and ethylene. *Science*. 2017;358(6366):1068-1071.
- Chi X, Li M, Di J, et al. A highly stable and flexible zeolite electrolyte solid-state Li-air battery. *Nature*. 2021;592:551-557.
- Guo Z, Li X, Hu S, Ye G, Zhou X, Coppens M-O. Understanding the role of internal diffusion barriers in Pt/beta zeolite catalyzed isomerization of n-heptane. *Angew Chem Int Ed*. 2020;132(4):1564-1567.
- Liu C, Su J, Liu S, et al. Insights into the key factor of zeolite morphology on the selective conversion of syngas to light aromatics over a Cr₂O₃/ZSM-5 catalyst. *ACS Catal*. 2020;10(24):15227-15237.
- Fasano M, Humplik T, Bevilacqua A, et al. Interplay between hydrophilicity and surface barriers on water transport in zeolite membranes. *Nat Commun*. 2016;7:1-8.
- Liang B, Zhang X, Xie Y, et al. An ultramicroporous metal-organic framework for high sieving separation of propylene from propane. *J Am Chem Soc*. 2020;142(41):17795-17801.
- Nag S, Ananthakrishna G, Maiti PK, Yashonath S. Separating hydrocarbon mixtures by driving the components in opposite directions: high degree of separation factor and energy efficiency. *Phys Rev Lett*. 2020;124(25):255901.
- Kärger J, Ruthven DM. Diffusion in nanoporous materials: fundamental principles, insights and challenges. *New J Chem*. 2016;40(5):4027-4048.
- Krishna R. Diffusion in porous crystalline materials. *Chem Soc Rev*. 2012;41(8):3099-3118.
- Rao SM, Saraçi E, Gläser R, Coppens M-O. Surface barriers as dominant mechanism to transport limitations in hierarchically structured catalysts—application to the zeolite-catalyzed alkylation of benzene with ethylene. *Chem Eng J*. 2017;329:45-55.
- Peng S, Gao M, Li H, Yang M, Ye M, Liu Z. Control of surface barriers in mass transfer to modulate methanol-to-olefins reaction over SAPO-34 zeolites. *Angew Chem Int Ed*. 2020;132(49):22129-22132.
- Peng S, Li H, Liu W, et al. Reaction rate enhancement by reducing surface diffusion barriers of guest molecules over ZSM-5 zeolites: a structured illumination microscopy study. *Chem Eng J*. 2022;430:132760.
- Newsome DA, Sholl DS. Predictive assessment of surface resistances in zeolite membranes using atomically detailed models. *J Phys Chem B*. 2005;109(15):7237-7244.
- Zimmermann NE, Zabel TJ, Keil FJ. Transport into nanosheets: diffusion equations put to test. *J Phys Chem C*. 2013;117(14):7384-7390.
- Liu L, Nicholson D, Bhatia SK. Interfacial resistance and length-dependent transport diffusivities in carbon nanotubes. *J Phys Chem C*. 2016;120(46):26363-26373.
- Sastre G, Kärger J, Ruthven DM. Surface barriers and symmetry of adsorption and desorption processes. *Adsorption*. 2021;27(5):777-785.
- Heinke L, Gu Z, Wöll C. The surface barrier phenomenon at the loading of metal-organic frameworks. *Nat Commun*. 2014;5(1):1-6.
- Karwacki L, Kox MH, Matthijs de Winter D, et al. Morphology-dependent zeolite intergrowth structures leading to distinct internal and outer-surface molecular diffusion barriers. *Nat Mater*. 2009;8(12):959-965.
- Sastre G, Jr K, Ruthven DM. Molecular dynamics study of diffusion and surface permeation of benzene in silicalite. *J Phys Chem C*. 2018;122(13):7217-7225.
- Heinke L, Kärger J. Correlating surface permeability with intracrystalline diffusivity in nanoporous solids. *Phys Rev Lett*. 2011;106(7):074501.
- Heinke L, Tzoulaki D, Chmelik C, et al. Assessing guest diffusivities in porous hosts from transient concentration profiles. *Phys Rev Lett*. 2009;102(6):065901.
- Hibbe F, Caro J, Chmelik C, et al. Monitoring molecular mass transfer in cation-free nanoporous host crystals of type AIPO-LTA. *J Am Chem Soc*. 2012;134(18):7725-7732.
- Kärger J, Binder T, Chmelik C, et al. Microimaging of transient guest profiles to monitor mass transfer in nanoporous materials. *Nat Mater*. 2014;13(4):333-343.
- Remi JCS, Lauerer A, Chmelik C, et al. The role of crystal diversity in understanding mass transfer in nanoporous materials. *Nat Mater*. 2015;15(4):401-406.
- Hibbe F, Chmelik C, Heinke L, et al. The nature of surface barriers on nanoporous solids explored by microimaging of transient guest distributions. *J Am Chem Soc*. 2011;133(9):2804-2807.
- Pinilla-Herrero I, Olsbye U, Márquez-Álvarez C, Sastre E. Effect of framework topology of SAPO catalysts on selectivity and deactivation profile in the methanol-to-olefins reaction. *J Catal*. 2017;352:191-207.
- Teixeira AR, Qi X, Chang C-C, Fan W, Conner WC, Dauenhauer PJ. On asymmetric surface barriers in MFI zeolites revealed by frequency response. *J Phys Chem C*. 2014;118(38):22166-22180.
- Combariza AF, Sastre G. Influence of zeolite surface in the sorption of methane from molecular dynamics. *J Phys Chem C*. 2011;115(28):13751-13758.

32. Zimmermann NE, Balaji SP, Keil FJ. Surface barriers of hydrocarbon transport triggered by ideal zeolite structures. *J Phys Chem C*. 2012;116(5):3677-3683.
33. Gao M, Li H, Yang M, et al. Direct quantification of surface barriers for mass transfer in nanoporous crystalline materials. *Commun Chem*. 2019;2(1):1-10.
34. Eic M, Ruthven DM. Diffusion of linear paraffins and cyclohexane in NaX and 5A zeolite crystals. *Zeolites*. 1988;8(6):472-479.
35. Eic M, Ruthven DM. A new experimental technique for measurement of intracrystalline diffusivity. *Zeolites*. 1988;8(1):40-45.
36. Brandani S, Mangano E. The zero length column technique to measure adsorption equilibrium and kinetics: lessons learnt from 30 years of experience. *Adsorption*. 2021;27(3):319-351.
37. Verbraeken M, Centineo A, Canobbio L, Brandani S. Accurate blank corrections for zero length column experiments. *Adsorption*. 2021;27:129-145.
38. McIntyre SR, Hunter-Sellers E, Saenz-Cavazos PA, Houghton AR, Williams DR. Novel zero-length column analysis of desorption curves for single cylindrical pellets. *Powder Technol*. 2023;416:118207.
39. Duong DD. *Adsorption Analysis: Equilibria and Kinetics*. Imperial College Press; 1998.
40. Hu S, Liu J, Ye G, Zhou X, Coppens M-O, Yuan W. Effect of external surface diffusion barriers on Pt/beta catalyzed isomerization of n-pentane. *Angew Chem Int Ed*. 2021;60(26):14394-14398.
41. Ruthven DM, Vidoni A. ZLC diffusion measurements: combined effect of surface resistance and internal diffusion. *Chem Eng Sci*. 2012;71:1-4.
42. Fick A. Ueber diffusion. *Ann Phys*. 1855;170(1):59-86.
43. Crank J. *The Mathematics of Diffusion*. Oxford University Press; 1979.
44. Carslaw H, Jaeger J. *Conduction of Heat in Solids*. Clarendon Press; 1975.
45. Tan J, Liu Z, Bao X, et al. Crystallization and Si incorporation mechanisms of SAPO-34. *Microporous Mesoporous Mater*. 2002;53(1-3):97-108.
46. Bonilla MR, Titze T, Schmidt F, et al. Diffusion study by IR micro-imaging of molecular uptake and release on mesoporous zeolites of structure type CHA and LTA. *Materials*. 2013;6(7):2662-2688.
47. Peng S, Xie Y, Wang L, et al. Exploring the influence of inter-and intra-crystal diversity of surface barriers in zeolites on mass transport by using super-resolution microimaging of time-resolved guest profiles. *Angew Chem Int Ed*. 2022;134(30):e202203903.
48. Bukowski BC, Keil FJ, Ravikovitch PI, Sastre G, Snurr RQ, Coppens M-O. Connecting theory and simulation with experiment for the study of diffusion in nanoporous solids. *Adsorption*. 2021;27:683-760.
49. Rajappa C, Krause C, Borah B, et al. Diffusion of pentane isomers in faujasite-type zeolites: NMR and molecular dynamics study. *Microporous Mesoporous Mater*. 2013;171:58-64.
50. Schuring D. *Diffusion in Zeolites: Towards a Microscopic Understanding*. Eindhoven University of Technology; 2004.
51. Cai D, Cui Y, Jia Z, Wang Y, Wei F. High-precision diffusion measurement of ethane and propane over SAPO-34 zeolites for methanol-to-olefin process. *Front Chem Sci Eng*. 2018;12(1):77-82.

SUPPORTING INFORMATION

Additional supporting information can be found online in the Supporting Information section at the end of this article.

How to cite this article: Xie Y, Li H, Lou C, Ye M, Liu Z. Quantifying molecular surface barriers and intracrystalline diffusion in nanoporous materials by zero-length column. *AIChE J*. 2023;69(10):e18159. doi:10.1002/aic.18159